Dynamic Range, Stability, and Fault-Tolerant Capability of Finite-Precision RLS Systolic Array Based on Givens Rotations

KouJuey Ray Liu, *Member, IEEE*, Shih-Fu Hsieh, *Member, IEEE*, Kung Yao, *Member, IEEE*, and Ching-Te Chiu

Abstract—**The QRD RLS algorithm is generally recognized as having good numerical properties under a finite-precision implementation. Furthermore, it is quite suited for VLSI implementation since it can be easily mapped onto a systolic array. However, it is still unclear how to obtain the dynamic range of the algorithm in order a wordlength can be chosen to ensure correct operations of the algorithm. In this paper, we first propose a quasi-steady state model by observing the rotation parameters generated by boundary cells will eventually reach *quasi-steady-state* regardless of the input data statistics if λ is close to one. With this model, we can obtain upper bounds of the dynamic range of processing cells. Thus the wordlength can be obtained from upper bounds of the dynamic range to prevent overflow and to ensure correct operations of the QRD RLS algorithm. Then we reconsider the stability problem under quantization effects with a more general analysis and obtain tighter bounds than given in a previous work [13]. Finally, two fault-tolerant problems, the missing error detection and the false alarm effect, that arise under finite-precision implementation are considered. Detailed analysis on preventing missing error detection with a false alarm free condition is presented.**

I. Introduction

LEAST-SQUARES (LS) problems have been an integral part of modern signal processing and communications applications, such as adaptive filtering, beamforming, array signal processing, channel equalization, etc. Efficient implementation of the recursive LS (RLS) algorithm is desirable to meet the high throughput and speed requirement of modern signal processing. Among many techniques to implement the RLS algorithm, the QR decomposition (QRD) RLS algorithm is one of the most promising algorithms in that it is numerical stable as well as suitable for parallel processing implementation in a systolic array [1], [8]. Gentleman and Kung [6] have proposed a QRD triangular systolic array based on Givens rotation, and McWhirter [21] used the systolic array to implement the QRD RLS algorithm efficiently. Since then, many researchers have considered and proposed various RLS algorithms (either constrained or non-constrained) based on methods such as the Givens rotation, modified Gram-Schmidt, and the Householder transformation for parallel processing architectures [3], [4], [9], [10], [14], [17], [22], [29]. Applications of the QR-based techniques to the least-square lattice algorithms have also been considered in [23]–[26]. In [15] and [16], Anfinson *et al.* and Liu and Yao have proposed efficient algorithm-based fault-tolerant schemes that can be easily incorporated with the QRD RLS systolic array. An error resulting from a temporary or permanent faulty cell can be detected in real-time, and the faulty cell can be reconfigurated out of service to prevent future contamination of the array. This makes the systolic implementation of the RLS algorithm more attractive in the practical real-time applications. In the United Kingdom, at STC Technology Ltd. (STL) in collaboration with Royal Signal and Radar Establishment (RSRE), a test bed of the QRD RLS systolic array has been built for radar applications [20]. Furthermore, this class of systolic array architectures can be used to solve SVD and eigenvalue problems [5], [18] that are the heart of many signal processing applications, such as high-resolution spectral estimation, direction-of-arrivals problems, and speech/image processing.

An important problem that needs to be resolved is the dynamic range of the QRD RLS systolic algorithm. Without knowing the dynamic range of an algorithm, we are unable to predict the wordlength (number of bits per word) required to ensure correct operations. Furthermore, the wordlength of an algorithm is one of the most crucial factors in designing hardware and circuits [27], since the wordlength affects the hardware complexity. Usually, shorter arithmetic wordlength leads to an implementation with smaller and faster hardware [27]. At the same time, we also do not want overflow to happen during the computation. Unfortunately, the dynamic range

Manuscript received October 4, 1990; revised January 28, 1991. This work was supported in part by NSF Grants ECD-8803012-06 and NCR-8814407, and by a UC Microgrant. This paper was recommended by Associate Editor K. K. Parhi.

K. J. R. Liu and C. T. Chiu are with the Electrical Engineering Department, Systems Research Center, University of Maryland, College Park, MD 20742.

S. F. Hsieh is with the Department of Communication Engineering, National Chiao Tung University, Hsinchu, Taiwan 30039.

K. Yao is with the Electrical Engineering Department, University of California, Los Angeles, CA 90024-1594.

IEEE Log Number 9143697.

0098-4094/91/0600-0625$01.00 ©1991 IEEE

of the QRD RLS algorithm is still unclear. While some simulations using finite wordlength have been presented in [23], both systolic array and lattice implementation are considered in this simulation study.

In this paper, we first observe that the cosine parameters generated by boundary cells will eventually reach *quasi-steady-state* if λ is close to one, which is the usual case. We will show that the quasi-steady-state and ensemble values of sine and cosine parameters are the same for all boundary cells. It is independent of the statistics of the input data sequence and the position of the boundary cell that generates the sine and cosine parameters. Simulation results are presented to support this observation. These results yield the tools needed to further investigate many properties of the QRD RLS systolic algorithm. Then, we can obtain upper bounds of the dynamic range of processing cells. Thus lower bounds on the wordlength can be obtained from upper bounds of the dynamic range to prevent overflow and to ensure correct operations of the QRD RLS algorithm.

Although the QRD RLS algorithm is generally recognized as having good numerical properties such as numerical stability under finite-precision implementation [1], [13], there is no mathematical proof of this until a recent paper by Leung and Haykin [13]. With the above results, we reconsider the stability problem under quantization effects with a more general analysis and obtain tighter bounds than given in previous work [13].

Given a finite wordlength, the computational precision is thus limited. Two important factors of the fault-tolerant capability, the *missing error detection* and the *false alarm* effects, resulting from the finite-precision implementation, are also considered in this paper. Basically, this is a trade-off issue. We will find a system that is capable of detecting any given small error size without having a false alarm problem.

The organization of this paper is as follows. First, a brief review of the fault-tolerant QRD RLS systolic array is given in Section II. Then, quasi-steady-state of the rotation parameters is discussed in Section III. Dynamic range and lower bound on wordlength are derived in Section IV. Stability and quantization effects are considered in Section V. Finally, the fault-tolerant capability is presented in Section VI and conclusion is given in Section VII.

II. Fault-Tolerant QRD RLS Systolic Array

Without computing weight vector explicitly, the systolic implementation of the QRD RLS algorithm proposed by McWhirter [21] can obtain the optimal residuals efficiently. The systolic array is shown in Fig. 1. It consists of two parts: a triangular array for computing QRD and a linear column array (denoted the response array (RA)) for computing the LS residual. One of the major features of the array is that multiple RA's can be added to obtained optimal residuals for multiple desired responses.

In [15], Liu and Yao proposed a real-time concurrent error detection scheme for this systolic array based on the algorithm-based fault-tolerance [2], [11]. The basic idea is that since the residuals of different desired responses can be computed simultaneously, an artificial desired response can be designed to detect an error produced by a faulty processor. In [15], it was shown that if the artificial desired response is designed as some proper combinations of the input data, the output residual of the system

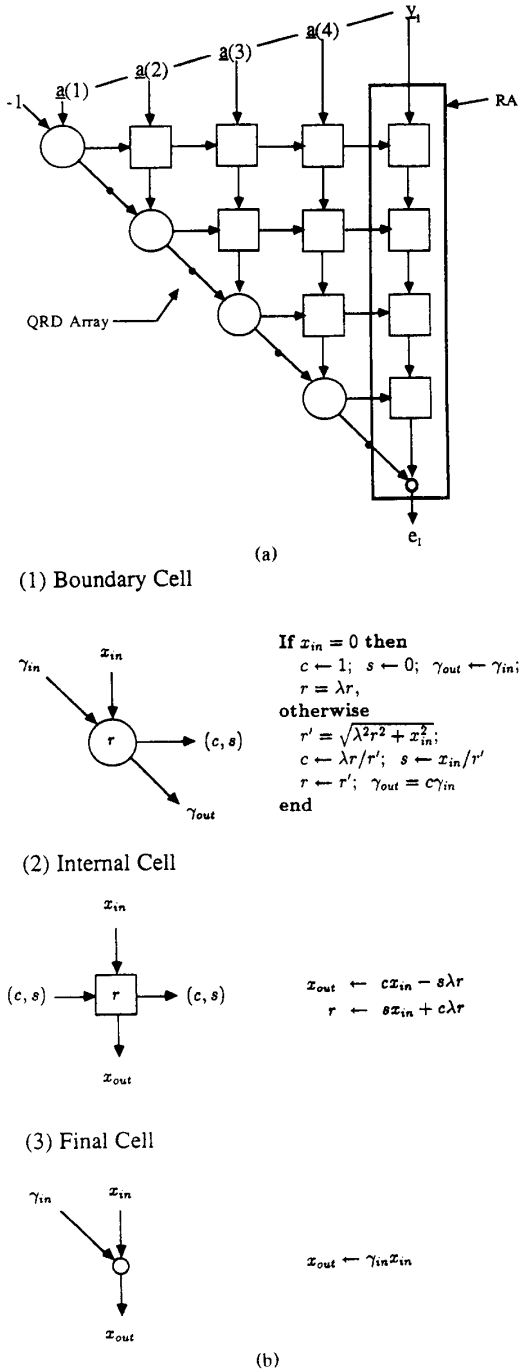

Fig. 1. (a) QRD RLS systolic array using Givens rotation method (b) Processing cells of the Givens rotation method.

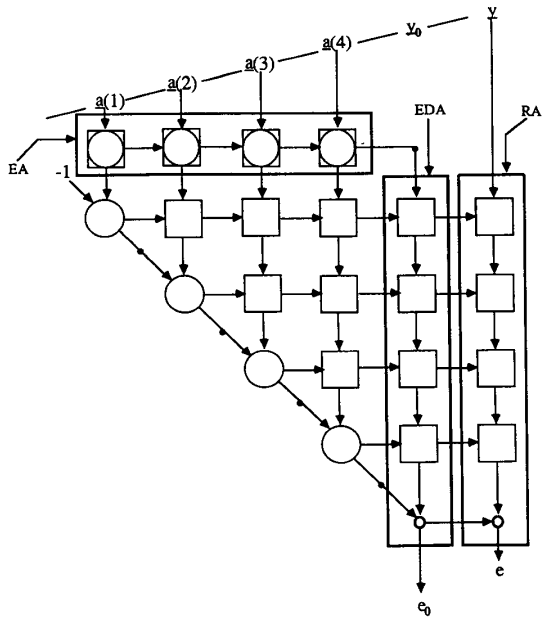

Fig. 2. Fault-tolerant QRD RLS systolic array.

will be zero if there is no fault. However, any occurring fault in the system will cause the residual to be nonzero and the fault can be detected in real-time. The fault-tolerant QRD RLS systolic array is shown in Fig. 2. As we can see, above the QRD triarray, a horizontal linear array called *encoding array*, is used to add up the incoming row (the checksum) to be the artificial desired response. The processing cell of the encoding array is an adder that adds both inputs and passes to the next cell. The artificial desired response then serves as the input to the new RA called *error detection array* (EDA) at the right side of the QRD triarray. The output of the EDA, e_0, now serves as the error detector. If there is no error, e_0 will always be zero. Whenever there is a faulty cell occurs during the computation, the error generated by the faulty cell will cause $e_0 \neq 0$ and thus the error is detected in real-time [15]. In [16], a similar work was proposed independently by Anfinson *et al.* based on the checksum encoding point of view as considered in [11].

All of these results are based on the assumption that the computation is infinite precision. Under finite-precision computation, there are two major effects: the missing error detection and false alarm effects, which will be considered in Section VI.

III. Quasi-Steady-State Model

From the updated recursive equation of the boundary cell (see Fig. 1), we have

$$r^2(k+1) = \lambda^2 r^2(k) + x^2(k) = \sum_{i=0}^{k} \lambda^{2i} x^2(k-i) \quad (1)$$

where $0 < \lambda \leqslant 1$ is the exponentially forgetting factor [8]. Assume the input sequence $\{x\}$ is zero-mean with variance σ^2; the expected value of $r^2(k+1)$ is given by

$$E\left[r^2(k+1)\right] = \sum_{i=0}^{k} \lambda^{2i} E\left(x^2(k-i)\right) = \sigma^2 \frac{1-\lambda^{2(k+1)}}{1-\lambda^2}. \quad (2)$$

When k is very large,

$$\lim_{k\to\infty} E\left[r^2(k)\right] = \frac{\sigma^2}{1-\lambda^2}. \quad (3)$$

Since $\sqrt{\cdot}$ is a concave function, from Jensen's inequality [28]

$$\lim_{k\to\infty} E(r(k)) \leqslant \lim_{k\to\infty} \sqrt{E\left[r^2(k)\right]} = \frac{\sigma}{\sqrt{1-\lambda^2}} \quad (4)$$

and from (1)

$$\frac{|x_{\min}|}{\sqrt{1-\lambda^2}} \leqslant \lim_{k\to\infty} r(k) \leqslant \frac{|x_{\max}|}{\sqrt{1-\lambda^2}} \quad (5)$$

where $|x_{\max}|$ and $|x_{\min}|$ are the maximum and minimum values of the sequence $\{|x|\}$.

The cosine parameter of the Givens rotation is computed by $c(k+1) = \lambda r(k)/r(k+1)$. The steady-state of this parameter exists if $\lim_{k\to\infty} c(k)$ exists. For the sequence $\{c(\cdot)\}$ to have a steady state, we need $\lim_{k\to\infty} r(k)/r(k+1) = \alpha$, where α is a constant. If $\alpha < 1$, then the sequence $\{r(\cdot)\}$ is unbounded, which conflicts with (5) which indicates $\{r(\cdot)\}$ should be bounded; if $\alpha > 1$, then $\lim_{k\to\infty} r(k) = 0$ which, again, conflicts with (5). Therefore, α has to be a unity to guarantee the steady state of $\{c(\cdot)\}$ exists. That is,

$$\lim_{k\to\infty} \frac{r(k)}{r(k+1)} = 1 \quad (6)$$

and the steady-state value of cosine, if it exists, is

$$\lim_{k\to\infty} c(k) = \lim_{k\to\infty} \frac{\lambda r(k-1)}{r(k)} = \lambda. \quad (7)$$

From (1), we can see that if $\lambda = 1$, then $\lim_{k\to\infty} r(k) \to \infty$ such that $\lim_{k\to\infty} r(k)/r(k+1) = 1$. In this case, though the steady-state of $\{c(\cdot)\}$ exists, $\{r(\cdot)\}$ is unbounded. Usually λ is chosen between .99 and 1, which is very close to one.[1] When we update $r(k)$ to $r(k+1)$ using (1), a λ portion of $r(k)$ is forgotten and an input $x(k)$ is added into it. If λ is close to one, when k is very large, $r(k)$ will come close to $r(k+1)$ and the input $x(k)$ plays a less and less significant role in computing $r(k+1)$. Then, it is obvious that

$$\lim_{k\to\infty} Er(k) = \lim_{k\to\infty} Er(k+1).$$

Therefore, from the averaging principle [19], which has been used successfully in many situations, the expected

[1]For different expressions as in [8], [13], and [21], λ is between .98 and 1.

cosine can be approximated by

$$\lim_{k\to\infty} Ec(k) \simeq \lambda \frac{Er(k-1)}{Er(k)} = \lambda. \tag{8}$$

When λ is close to one, from above discussions, we have

$$\lim_{k\to\infty} c(k) = \lim_{k\to\infty} \frac{\lambda r(k)}{r(k+1)} = \lambda + \delta(\lambda, x) \tag{9}$$

where $\delta(\lambda, x)$ represents the small deviation due to the forgotten λ portion of r and input of x. If δ is very small such that it is negligible when k is large, we say that the sequence $\{c(\cdot)\}$ has reached the *quasi-steady-state*.

Generally, it is difficult to quantitatively characterize $\delta(\lambda, x)$. Simulations will be used to demonstrate the smallness of δ. Here we model the input signal sequence $\{x\}$ to the systolic array as a second-order AR process described by

$$x(n) + a_1 x(n-1) + a_2 x(n-2) = v(n) \tag{10}$$

where $v(n)$ is a white Gaussian noise process of zero-mean and unit variance. Choice of different AR parameters a_1 and a_2 will give us different stationary and nonstationary realizations of the AR process [8, chap. 2]. In our simulations, three different categories of signal are encountered. The first category consists of three stationary AR processes given by AR1 ($a_1 = -0.1$, $a_2 = -0.8$), AR2 ($a_1 = 0.1$, $a_2 = -0.8$) with real roots, and AR3 ($a_1 = -0.975$, $a_2 = 0.95$) with complex-conjugate roots. The second category yields a nonstationary AR process, AR4 ($a_1 = -0.6$, $a_2 = -0.5$), and the third category is a white Gaussian noise process, WN, with zero mean and unit variance. All of the AR processes are normalized to unit variance. Table I shows the mean of the cosine parameters for different input data with different λ values. This table justifies the result in (8). Table II shows the variance of δ for different input data with different λ values. The values of those variances are on the order of 10^{-4} to 10^{-6}, which implies that δ is indeed very small. They can be closely approximated by using quadratic polynomials as follows:

$$\text{AR1: } \sigma_\delta^2(\lambda) = 1.5938 - 3.182\lambda + 1.5882\lambda^2$$

$$\text{AR2: } \sigma_\delta^2(\lambda) = 1.5991 - 3.1919\lambda + 1.5928\lambda^2$$

$$\text{AR3: } \sigma_\delta^2(\lambda) = 1.5812 - 3.1595\lambda + 1.5784\lambda^2$$

$$\text{AR4: } \sigma_\delta^2(\lambda) = 1.4492 - 2.8936\lambda + 1.4444\lambda^2$$

$$\text{AR5: } \sigma_\delta^2(\lambda) = 1.6437 - 3.2904\lambda + 1.6431\lambda^2 \tag{11}$$

where $0.98 \leqslant \lambda < 1$.

While the statistics of the input data are different, the variances can be described by λ in similar manners (see Fig. 3). This means that when λ is close to one and the quasi-steady-state is reached, the size of the variation δ is mainly governed by λ instead of the statistics of the input data. Fig. 3 shows the plots of the variances on a decibel scale.

From these results, we conclude that the sequence $\{c(\cdot)\}$ reaches the quasi-steady-state regardless of the input statistics if λ is close to one. Thus we can write

$$\lim_{k\to\infty} c(k+1) \simeq \lim_{k\to\infty} Ec(k+1) \simeq \lambda,$$

$$\lim_{k\to\infty} s(k+1) \simeq \lim_{k\to\infty} Es(k+1) \simeq \sqrt{1-\lambda^2}. \tag{12}$$

TABLE I
MEAN VALUES OF THE COSINE PARAMETERS FOR DIFFERENT INPUT SIGNALS

	AR1	AR2	AR3	AR4	WN
$\lambda = .980$	.9800	.9800	.9802	.9799	.9801
$\lambda = .985$	.9849	.9849	.9851	.9848	.9850
$\lambda = .990$	.9897	.9897	.9900	.9897	.9899
$\lambda = .991$	.9907	.9907	.9910	.9907	.9909
$\lambda = .993$	.9927	.9927	.9930	.9927	.9929
$\lambda = .995$	.9947	.9947	.9950	.9947	.9949
$\lambda = .997$	.9967	.9967	.9970	.9967	.9969
$\lambda = .999$	.9985	.9985	.9987	.9985	.9986

TABLE II
VARIANCES OF THE δ FOR DIFFERENT INPUT SIGNALS

	AR1	AR2	AR3	AR4	WN
$\lambda = .980$	7.3885e-4	7.5465e-4	6.8163e-4	6.6721e-4	7.3367e-4
$\lambda = .985$	4.3970e-4	4.5144e-4	3.9577e-4	3.9517e-4	4.3308e-4
$\lambda = .990$	2.0903e-4	2.1463e-4	1.8376e-4	1.8918e-4	2.0080e-4
$\lambda = .991$	1.7154e-4	1.7875e-4	1.4883e-4	1.5562e-4	1.6659e-4
$\lambda = .993$	1.0991e-4	1.1390e-4	9.1016e-4	9.6440e-5	1.0323e-4
$\lambda = .995$	5.9724e-5	6.0796e-5	4.6789e-5	5.1856e-5	5.3525e-5
$\lambda = .997$	2.3007e-5	2.4735e-5	1.6808e-5	1.9908e-5	2.0504e-5
$\lambda = .999$	4.1127e-6	3.1590e-6	3.5167e-6	4.3511e-6	4.6490e-6

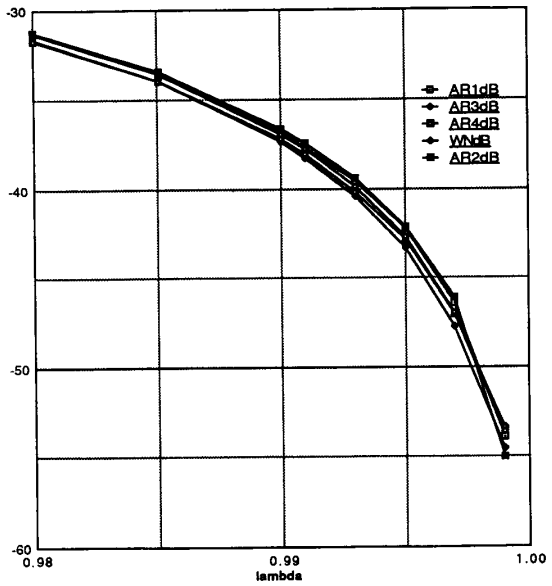

Fig. 3. Plots of variances in decibel scale.

The quasi-steady-state and ensemble values of sine and cosine parameters are the same for all boundary cells. It is independent of the statistics of the input data sequence and the position of the boundary cell which generates the sine and cosine parameters. These results yield the tools needed to investigate further many properties of the QRD RLS systolic algorithm.

IV. Dynamic Range and Lower Bound on Wordlength

Denote PE_{ij} as the (i,j) processing cell of the array. From Fig. 1, the dynamic range of the content of the boundary cell PE_{11} can be upper bounded by

$$\lim_{k\to\infty} r_{11}^2(k+1) = \lim_{k\to\infty} \sum_{i=0}^{k} \lambda^{2i} x^2(k-i) \leqslant \lim_{k\to\infty} x_{\max}^2 \sum_{i=0}^{k} \lambda^{2i} = \frac{x_{\max}^2}{1-\lambda^2}. \quad (13)$$

Therefore,

$$\lim_{k\to\infty} |r_{11}(k)| \leqslant \frac{|x_{\max}|}{\sqrt{1-\lambda^2}} \triangleq \Re. \quad (14)$$

From the definition of the cosine parameter as given in Fig. 1, we can see that it is always non-negative. For internal cell PE_{1j} (of the first row), we have

$$\begin{aligned} |r_{1j}(k+1)| &= |s(k)x(k) + c(k)\lambda r_{1j}(k)| \\ &= \big|s(k)x(k) + c(k)\lambda[s(k-1)x(k-1) \\ &\quad + c(k-1)\lambda r_{1j}(k-1)]\big| \\ &\leqslant \sum_{i=0}^{k} \lambda^i |x(k-i)s(k-i)| \prod_{l=0}^{i-1} c(k-l) \\ &\leqslant |x_{\max}| \sum_{i=0}^{k} \lambda^i |s(k-i)| \prod_{l=0}^{i-1} c(k-l). \end{aligned} \quad (15)$$

From the basic relationship between the geometric mean and the arithmetic mean, we know

$$\left(\frac{a_1 + a_2 + \cdots + a_n}{n}\right)^n \geqslant a_1 \cdot a_2 \cdots a_n. \quad (16)$$

If n is large enough, then from the law of large numbers, we know

$$\lim_{n\to\infty} \frac{a_1 + a_2 + \cdots + a_n}{n} \to E(a).$$

Therefore,

$$E(a)^n \geqslant \prod_{i=1}^{n} a_i$$

when n is large. We can further simplify the bound for $k \to \infty$ by using this inequality as follows:

$$\begin{aligned} &\lim_{k\to\infty} |r_{1j}(k+1)| \\ &\quad \leqslant |x_{\max}| \lim_{k\to\infty} \sum_{i=0}^{k} \lambda^i |s(k-i)| E(c(k-i))^i \\ &\quad \simeq |x_{\max}| \lim_{k\to\infty} \sum_{i=0}^{k} \lambda^{2i} \cdot \sqrt{1-\lambda^2} = \frac{|x_{\max}|}{\sqrt{1-\lambda^2}} = \Re. \end{aligned} \quad (17)$$

From (14) and (17), we can see the steady-state dynamic range of the first row is upper bounded by $\Re$ for both boundary and internal cells. The dynamic range of the second row depends on the output of internal cells of the first row. Denote the output of the first row as x_{out}. From Fig. 1, we have

$$x_{\text{out}}(k+1) = c(k)x(k) - s(k)\lambda r(k). \quad (18)$$

The first term on the right-hand side of (18) can be bounded by

$$\lim_{k\to\infty} |c(k)x(k)| \leqslant \lambda |x_{\max}| \quad (19)$$

and from (17) the second term is bounded by

$$\lim_{k\to\infty} |s(k)\lambda r(k)| \leqslant \sqrt{1-\lambda^2} \cdot \lambda \frac{|x_{\max}|}{\sqrt{1-\lambda^2}} = \lambda |x_{\max}|. \quad (20)$$

There are two possible cases.

Case 1) Highly fluctuated input: The value of $x(k)$ may vary differently from time to time such that for most of the time, $s(k)r(k)$ may have the opposite sign of $x(k)$. For this case

$$\lim_{k\to\infty} |x_{\text{out}}(k)| \leqslant 2\lambda |x_{\max}|. \quad (21)$$

Case 2) Smooth input: For this case, the input data sequence does not change its value rapidly, and therefore, $s(k)r(k)$ may have the same sign as $x(k)$ for most of the time. The bound is

$$\lim_{k\to\infty} |x_{\text{out}}(k)| \leqslant \lambda |x_{\max}|. \quad (22)$$

From (14) and (17), it is obvious the steady-state dynamic range of the second row is bounded by

$$\lim_{k\to\infty} |r_{2j}(k)| \leqslant \frac{2\lambda |x_{\max}|}{\sqrt{1-\lambda^2}} = 2\lambda\Re \quad (23)$$

for the highly fluctuating input, and

$$\lim_{k\to\infty} |r_{2j}(k)| \leqslant \lambda\Re \quad (24)$$

for the smooth input. From the above results, the steady-state dynamic range of the mth row is bounded by

$$\lim_{k\to\infty} |r_{mj}(k)| \leqslant (2\lambda)^{m-1} \cdot \Re \quad (25)$$

for the highly fluctuating input and

$$\lim_{k\to\infty} |r_{mj}(k)| \leqslant (\lambda)^{m-1} \Re \quad (26)$$

for the smooth input. For Case 1, the dynamic range is increasing exponentially with a factor of 2λ, and for Case 2, decreasing exponentially with a factor of λ.

From (25) and (26), we can see that the dynamic range may increase or decrease with each row. Its behavior depends on the characteristics of the input signal. For a given row, its dynamic range may follow (25) for some periods (increasing) and then switch to (26) for some periods (decreasing). Either way, (25) represents the worst case scenario.

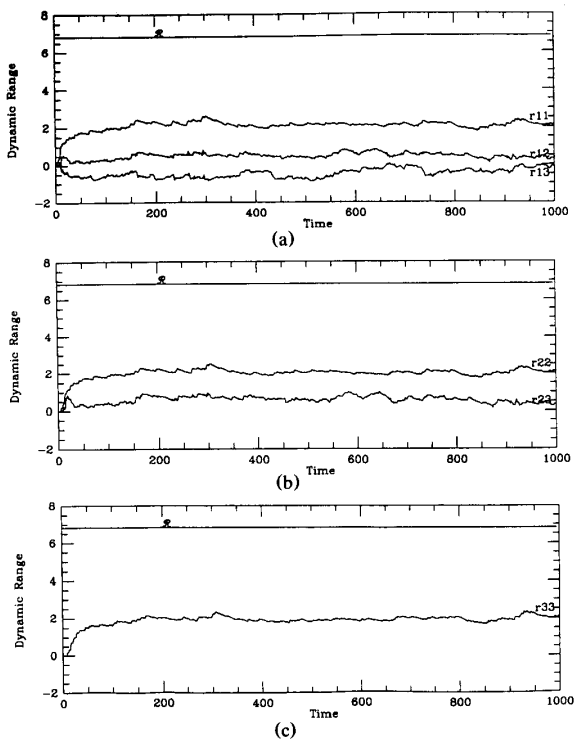

Fig. 4. Plots of the contents of processing cells with AR3 signal for $\lambda = 0.911$ and order $p = 3$. (a) First row. (b) Second row. (c) Third row.

Denote B_m as the wordlength of the mth row, to prevent outflow and to ensure the correct operation of the QRD RLS algorithm. Thus we require $2^{B_m} \geq (2\lambda)^{m-1}\Re$ for fixed-point operation, and therefore,

$$B_m \geq \lceil (m-1)(1+\log_2 \lambda) + \log_2 \Re \rceil. \quad (27)$$

For the fluctuating input, when $(2\lambda)^{n-1} = 2$, one more bit is needed for the wordlength of the following rows. The number of rows n for each bit increase is

$$n = \left\lfloor 1 + \frac{1}{1+\log_2 \lambda} \right\rfloor \quad (28)$$

which is a monotonically decreasing function of λ. If $\lambda \leq 0.5$, then no such n exists. That is, the wordlength of the array can be fixed at $\Re$ without the overflow problem. For smooth input, when $\lambda^{n-1} = (1/2)$, one bit can be discarded from the wordlength of the following rows. The number of rows n for each bit decrease is

$$n = \left\lceil 1 - \frac{1}{\log_2 \lambda} \right\rceil \quad (29)$$

which is a monotonically increasing function of λ. For $\lambda \leq 0.5$, $n = 2$. That is, for every two rows we can discard one bit for the wordlength.

Our simulations verified the above results. Here we provide some examples. Fig. 4 shows a simulation of the contents of internal and boundary cells of different rows as well as the upper bound $\Re$ under AR3 input signal for $\lambda = 0.991$ and $p = 3$. Table III compares the upper bound

TABLE III
COMPARISONS OF THE UPPER BOUND $\Re$ AND THE MAXIMUM VALUES OF THE CONTENTS OF THE BOUNDARY AND INTERNAL CELLS

	AR1	AR2	AR3	AR4
$\Re$	47.5737	16.6493	6.8209	17.1317
Max r_{ii}	12.1135	5.6755	2.5770	6.3590
Max r_{ij}	5.4948	3.3982	0.9036	4.2805

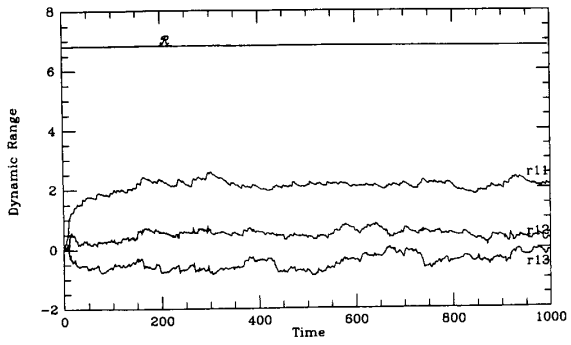

Fig. 5. Plots of the contents of the first row processing cells with finite wordlengths: 3 bits (row 1), 4 bits (row 2), 5 bits (row 3), and 4 bits for others.

$\Re$ and the maximum value of contents of boundary and internal cells for different input signals. From these, we can see that $\Re$ is a good upper bound for both boundary and internal cells. From (27), we can choose the minimum wordlengths for the AR3 input signal. We found that it needs three bits for the wordlength of the first row, four bits for the second row, and five bits for the third row. As shown in Fig. 5, the resultant contents are almost identical to those of Fig. 4, which is the result of a double-precision implementation.

V. Stability and Quantization Effect

In this section, we consider stability under the quantization effect. Here, the stability is defined in the sense of bounded input/bounded output (BIBO) as in [13]. From (21) and (22), the output of the mth row is bounded by

$$\lim_{k \to \infty} |x_{\text{out}_m}| \leq (2\lambda)^{m-1} |x_{\max}| \quad (30)$$

for the highly fluctuating input and

$$\lim_{k \to \infty} |x_{\text{out}_m}| \leq \lambda^{m-1} |x_{\max}| \quad (31)$$

for the smooth input.

The order of least-squares estimation p is always finite. The output of the last row of the QR triarray is bounded, in the worst case, by $\lim_{k \to \infty} |x_{\text{out}_p}| \leq (2\lambda)^{p-1} |x_{\max}|$. The residual is then asymptotically bounded by

$$\lim_{k \to \infty} |e(k)| = \lim_{k \to \infty} \gamma(k) |x_{\text{out}_p}(k)| \leq (2\lambda)^{p-1} |x_{\max}| \quad (32)$$

where $\gamma(k) = \prod_{i=1}^{p} c_i(k)$ and c_i's are the related cosine parameters [21]. Thus for $\lambda < 1$, if the input data are bounded, that is, $|x_{\max}| < \infty$, the output is always bounded.

The QRD RLS systolic array constitutes a BIBO stable system under unlimited precision implementation. Practically, the wordlength of each processing cell is finite-precision. Leung and Haykin [13] first considered the stability under this effect and showed the QRD RLS algorithm is stable under finite-precision implementation. Here we reconsider this problem and give a more general analysis and a tighter bound.

Denote $Q(\cdot)$ as the quantization operator and $\check{x}$ as the quantized value of x. Since the quantization error for the additions of quantized parameters is much smaller than that of multiplications, to make the analysis simpler, we express the quantization error for additions as

$$Q\left(\sum_{i=1}^{n}\check{a}_i\right)=\sum_{i=1}^{n}\check{a}_i+\delta_n. \tag{33}$$

From (1), the square of the quantized content of the boundary cell is

$$\begin{aligned}\check{r}^2(k+1)&=Q\big(Q(\check{\lambda}^2\check{r}^2(k))+Q(\check{x}^2(k))\big)\\&=\sum_{i=0}^{k}Q\big(\check{\lambda}^{2i}\check{x}^2(k-i)\big)+\delta_{k+1}.\end{aligned} \tag{34}$$

The quantization operator Q is a bounded operator such that $|Q(x)|\leqslant K|x|$ for all x and some K [13], (34) can be bounded by

$$\begin{aligned}|\check{r}^2(k+1)|&\leqslant K_0|\check{\lambda}^{2k}\check{x}^2(0)|+K_1|\check{\lambda}^{2(k-1)}\check{x}^2(1)|+\cdots\\&\quad+K_k|\check{x}^2(k)|+\delta_{k+1}\\&\leqslant K_{\max}\cdot\check{x}^2_{\max}(1+\check{\lambda}^2+\cdots+\check{\lambda}^{2k})\end{aligned} \tag{35}$$

where $\check{x}_{\max}$ is the maximum quantized value of sequence $\check{x}$. The asymptotic behavior can be obtained by taking the limit on both sides, and it becomes

$$\lim_{k\to\infty}|\check{r}^2(k)|\leqslant K_{\max}\cdot\check{x}^2_{\max}\frac{1}{1-\check{\lambda}^2}. \tag{36}$$

Therefore, the quantized content is given by

$$\begin{aligned}\lim_{k\to\infty}|\check{r}(k)|&=\lim_{k\to\infty}Q\left(\sqrt{\check{r}^2(k)}\right)\\&\leqslant K'_{\max}\frac{|\check{x}_{\max}|}{\sqrt{1-\check{\lambda}^2}}\triangleq K'_{\max}\check{\Re}.\end{aligned} \tag{37}$$

With the same arguments as in Section III, we then have

$$\lim_{k\to\infty}\frac{\check{r}(k)}{\check{r}(k+1)}\simeq 1 \tag{38}$$

if $\check{\lambda}$ is close to 1. The quantized steady-state value of cosine is

$$\lim_{k\to\infty}\check{c}(k+1)=\lim_{k\to\infty}\frac{\check{\lambda}\check{r}(k)}{\check{r}(k+1)}\simeq\check{\lambda} \tag{39}$$

and the quantized steady-state value of sine is

$$\lim_{k\to\infty}\check{s}(k+1)=Q\left(\sqrt{1-\check{\lambda}}\right).$$

Analogous to Section III, we can further obtain

$$\lim_{k\to\infty}E\check{c}(k)=\check{\lambda}\quad\text{and}\quad\lim_{k\to\infty}E\check{s}(k)=Q\left(\sqrt{1-\check{\lambda}}\right).$$

Now consider the quantized content of the internal cell from (15):

$$\begin{aligned}&|\check{r}_{1j}(k+1)|\\&\quad=|Q(Q(\check{s}(k)\check{x}(k))+Q(\check{c}(k)\check{\lambda}\check{r}(k))|\\&\quad=\sum_{i=0}^{k}Q\left(\check{\lambda}^i|\check{x}(k-i)\check{s}(k-i)|\prod_{j=0}^{i-1}\check{c}(k-j)\right)+\delta_{k+1}\\&\quad\leqslant K''_{\max}|\check{x}_{\max}|\sum_{i=0}^{k}\check{\lambda}^i|\check{s}(k-i)|\prod_{j=0}^{i-1}\check{c}(k-j)\end{aligned} \tag{40}$$

where $K''_{\max}$ results from quantization error that includes δ_{k+1}. From Section IV, (39), and (40), the quantized steady-state dynamic range of the internal cell is bounded by

$$\lim_{k\to\infty}|\check{r}_{1j}(k)|\leqslant K''_{\max}\frac{|\check{x}_{\max}|}{\sqrt{1-\check{\lambda}}}=K''_{\max}\check{\Re}. \tag{41}$$

The output of the mth row is bounded, under the quantization effect, by

$$\lim_{k\to\infty}|\check{r}_{1j}(k)|\leqslant K''_{\max}(2\check{\lambda})^{m-1}\check{\Re} \tag{42}$$

for the highly fluctuating input and

$$\lim_{k\to\infty}|\check{r}_{1j}(k)|\leqslant K''_{\max}(\check{\lambda})^{m-1}\check{\Re} \tag{43}$$

for smooth input.

From these results, the quantized asymptotic value of the residual can be obtained as

$$\lim_{k\to\infty}|\check{e}(k)|\leqslant K''_{\max}(2\check{\lambda})^{p-1}\check{\Re}. \tag{44}$$

Thus, if $\lambda<1$ and the input data are bounded, the QRD RLS systolic array constitutes a BIBO stable system under the quantization effect.

VI. Finite Wordlength Effects of Fault-Tolerant Capability

In this section, we discuss the finite-length effects of the fault-tolerant capability. The first problem is that of missing error detection that results from the cumulative multiplications of the cosine value with a small error. Since each $|c(k)|\leqslant 1$, the error will then be decreasing with time. With a finite-precision implementation, this may result in a failure of error detection. The minimum wordlength to circumvent this problem is then derived. The second problem is called the false alarm. With the quantization effects, the system without fault may produce quantization errors to cause a false alarm. A threshold device is then introduced to circumvent this problem.

6.1. Missing Error Detection

It is shown in Fig. 2 that the input to each column of the triangular QRD array is denoted as $\underline{a}(j)$, where j is the corresponding column, and $\underline{y}$ is the input to the RA

and $\underline{y}_0$ is the artificial desired response to the EDA. By *missing error detection*, we mean that a small error generated by a faulty processing cell is not detected due to the finite-precision computation. Assume a fault occurs in an internal cell PE_{ij}, $i \neq j$, at a faulty moment. The output of this faulty cell is thus erroneous and can be described by $x_{\text{out}}^{\epsilon} = x_{\text{out}} + \delta$, where x_{out} is the fault-free output and δ is the error generated by the fault. The error propagation path can be described by

$$PE_{ij} \rightarrow PE_{(i+1)j} \rightarrow \cdots \rightarrow PE_{jj}$$

and then PE_{kl}, $k \geq j$, $l \geq j$ are all contaminated [15]. From the operations executed by the internal cell, the error is modified to $c_{i+1}\delta$ by $PE_{(i+1)j}$ and the cumulative modifications of the error before reaching the boundary cell, PE_{jj}, is

$$\eta = \delta \prod_{k=i+1}^{j-1} c_k \tag{45}$$

where c_i is the cosine parameter generated by the boundary cell PE_{ii}. Let c_j' and s_j' denote the erroneous c_j and s_j, respectively. The c_j' and s_j' are then given by

$$c_j' = \frac{\lambda r}{\sqrt{\lambda^2 r^2 + (x_{\text{in}} + \eta)^2}}, \qquad s_j' = \frac{x_{\text{in}} + \eta}{\sqrt{\lambda^2 r^2 + (x_{\text{in}} + \eta)^2}}. \tag{46}$$

In this case, s_j' is no longer proportional to x_{in}, $\underline{a}(j)$ will not be zeroed by the jth cell of the EDA [15]. From the *principle of cancellation* that will be considered later, we know that for the artificial desired response, the data coming from the ith column were canceled by the ith cell of the EDA. Therefore, we can only focus on the generated error that will not be cancelled and eventually be propagated to other part of the array. The size of the error generated by the jth cell of the EDA can then be derived as

$$\eta_j = c_j' x_{\text{in}} - s_j' \lambda r = -\frac{\lambda r \eta}{\sqrt{r'^2 + 2\eta x_{in} + \eta^2}} = -c_j' \eta \tag{47}$$

where $r' = \sqrt{\lambda^2 r^2 + x_{\text{in}}^2}$ is the new updated and uncontaminated value of the content of PE_{jj}. When η_j propagates down to the output of the EDA, η_j is influenced by the contaminated cosines c' of each following row. The error output at e_0 due to an error δ generated at PE_{ij} is then given by

$$e_0^{\delta}(i,j) = -\gamma \prod_{m=j+1}^{p} c_m' \eta_j = -\gamma \prod_{m=j}^{p} c_m' \eta$$
$$= -\gamma \prod_{k=i+1}^{j-1} c_k \cdot \prod_{m=j}^{p} c_m' \delta \tag{48}$$

where $\gamma = \prod_{l=1}^{j-1} c_l \prod_{k=j}^{p} c_k'$ [21]. It becomes

$$e_0^{\delta}(i,j) = -\prod_{l=1}^{i} c_l \prod_{k=i+1}^{j-1} c_k^2 \prod_{m=j}^{p} c_m'^2 \delta. \tag{49}$$

Next, assume a fault occurs in a boundary cell, PE_{jj}, $1 \leq j \leq p$, at the faulty moment. Both erroneous c_j' and s_j' produced by PE_{jj} can be written by

$$c_j' = \frac{\lambda r + \delta_c}{r_{\epsilon}'}, \qquad s_j' = \frac{x_{\text{in}} + \delta_s}{r_{\epsilon}'} \tag{50}$$

where δ_c and δ_s represent errors in the numerators while r_{ϵ}' represents the erroneous content of the denominators of c_j and s_j. The error produced by the jth cell of the EDA is then given by

$$\eta_j = c_j' x_{\text{in}} - s_j' \lambda r = \frac{x_{\text{in}} \delta_c - \lambda r \delta_s}{r_{\epsilon}'} \tag{51}$$

and the output error at e_0 due to a faulty boundary cell is given by

$$e_0^{\delta}(j,j) = \gamma \prod_{m=j+1}^{p} c_m' \cdot \frac{x_{\text{in}} \delta_c - \lambda r \delta_s}{r_{\epsilon}'}$$
$$= \prod_{l=1}^{j} c_l \cdot \prod_{m=j+1}^{p} c_m'^2 \cdot \eta_j. \tag{52}$$

From (49) and (52), we can see that $e_0^{\delta} \neq 0$, under infinite precision condition, if a fault occurs in the system, except when $u_{\text{in}}\delta_c = \lambda r \delta_s$ in (51). However, this is unlikely to happen. From [15] and [21], we have $0 < c_i \leq 1$. The error may not be detected after multiple multiplications of c_i in (49) and (52) under finite-precision implementation. It is obvious there is no such problem when δ is large. Since r in (46) tends to be a large number asymptotically, it is reasonable to assume the error size δ generated by a fault is much smaller than r when δ is small. Under this circumstance, from (46), we have $c_j' \cong c_j$. In the quasi-steady-state, the asymptotic behavior of erroneous cosine is $c_j' \cong c_j = \lambda$. From (49) and (52), the error output e_0^{δ} due to an error size δ is then approximated by

$$e_0^{\delta}(i,j) \cong -\lambda^{2p-i}\delta \tag{53}$$

for a faulty internal cell and

$$e_0^{\delta}(j,j) \cong \lambda^{2p-j}\eta_j \tag{54}$$

for a faulty boundary cell. Let B_{Δ} be the wordlength of each memory and register of fixed point arithmetics. That is, each wordlength is of B_{Δ} bits and let $\Delta = \min(\delta, \eta_j)$. To ensure the detection of error size Δ, we need

$$\lambda^{2p-i}\Delta \geq \lambda^{2p}\Delta \geq 2^{-B_{\Delta}}. \tag{55}$$

Therefore, the wordlength should be at least

$$B_{\Delta} \geq \lceil -2p \log_2 \lambda - \log_2 \Delta \rceil \tag{56}$$

such that the small error size Δ can be detected. The second term of the right-hand size is obvious since the error size Δ must be detected; the first term is to account for the effects that the error propagates through the array of LS order p with forgetting factor λ.

We can verify the above result by the following example. A systolic array with order $p = 3$, $\lambda = 0.999$ has an error $\delta = 3 \cdot 10^{-4}$ occurring at the internal cell PE_{12} at time 25. Due to the asymptotic behavior of the cosine parameters, η_j can be approximated as $\eta_j = \lambda \cdot \delta = 2.997 \cdot$

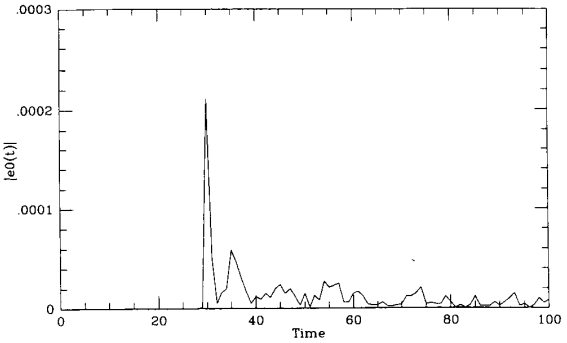

Fig. 6. The error size $\delta = 3 \cdot 10^{-4}$ occurring at PE_{12} can be detected for $B_\Delta = 12$.

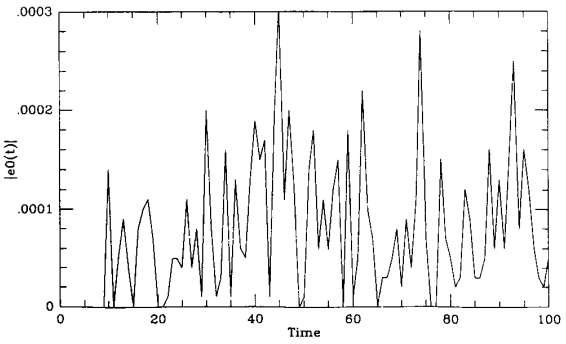

Fig. 7. The error size $\delta = 3 \cdot 10^{-4}$ occurring at PE_{12} cannot be detected for $B_\Delta = 5$.

10^{-4} and $\Delta = \eta_j$. From (56), we have $B_\Delta \geqslant 12$. Fig. 6 shows that the small error size can be detected for $B_\Delta = 12$ at time 30. However, as shown in Fig. 7 for a smaller wordlength of $B_\Delta = 5$, the error size that can be seen at the output becomes very small and is buried in the noise resulting from the quantization effects of small wordlength. The detector not only misses the error, but also causes the false alarm phenomenon that will be considered in the next subsection.

6.2. False Alarm

Due to the finite-precision implementation, the residual output of the EDA will not actual be zero even if there is no fault in the system. We call this effect a false alarm. Fig. 8 shows the false alarm problem for the above example with wordlength of 9 bits. Here, we are going to model and quantitatively describe the false alarm effect and introduce a threshold device to overcome this problem.

6.2.1. Cancellation Principle: Suppose now we have a fault-tolerant QRD RLS array of order $p = 3$. Denote the first and second rows of data input as $(x_1, x_2, x_3, x_1 + x_2 + x_3)$ and $(x_1', x_2', x_3', x_1' + x_2' + x_3')$, respectively, where the checksums $x_1 + x_2 + x_3$ and $x_1' + x_2' + x_3'$ are inputs to the EDA. After both data pass through the array,

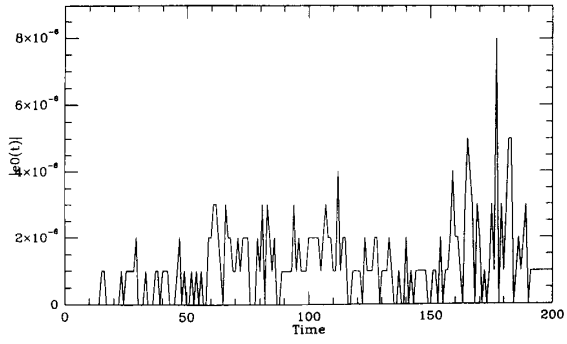

Fig. 8. False alarm effect for finite wordlength with 9-bit implementation.

according to the operations of the processing cells, the contents of the cells of the first row are

$$\begin{aligned} r_{11} &= \sqrt{x_1^2 + x_1'^2} \\ r_{12} &= sx_2' + cx_2 \\ r_{13} &= sx_3' + cx_3 \\ r_{14} &= s(x_1' + x_2' + x_3') + c(x_1 + x_2 + x_3) \end{aligned} \tag{57}$$

where $c = x_1 / r_{11}$ and $s = x_1' / r_{11}$ are the rotation parameters generated by the boundary cell and r_{ij} is the content of PE_{ij}. The output of the internal cells are

$$\begin{aligned} z_{12} &= cx_2' - sx_2 \\ z_{13} &= cx_3' - sx_3 \\ z_{14} &= c(x_1' + x_2' + x_3') - s(x_1 + x_2 + x_3). \end{aligned} \tag{58}$$

Since $sx_1' + cx_1 = \sqrt{x_1^2 + x_1'^2}$ and $cx_1' - sx_1 = 0$, we have $r_{14} = r_{11} + r_{12} + r_{13}$ and $z_{14} = z_{12} + z_{13}$. That is, both the contents and the outputs of the first row still meet the checksum. The outputs of the first cell of EDA, z_{14}, can be rewritten as

$$z_{14} = c(x_2' + x_3') - s(x_2 + x_3). \tag{59}$$

We can see that the data from the first column got cancelled out by the first cell of the EDA. Since the outputs meet the checksum, with the same principle, the data from the second column will get cancelled out by the second cell of the EDA. Thus this observation can be generalized and stated as below:

Cancellation Principle: With the checksum encoding data inputted to EDA, the data from the ith column was cancelled by the ith cell of the EDA. □

For a finite-precision implementation, due to the roundoff error, the data from the ith column will not be completely cancelled by the ith cell of the EDA. This effect results in the false alarm problem.

6.2.2. Finite-Precision Floating Point Error Model: A floating point number f can be represented by [7]

$$\begin{aligned} f &= \pm .d_1 d_2 \cdots d_t \times \beta^e, \\ & 0 \leqslant d_i < \beta, \quad d_1 \neq 0, \quad L \leqslant e \leqslant U \end{aligned} \tag{60}$$

where β is the base, t is the precision, and $[L, U]$ is the exponent range. The floating point operator fl can be

TABLE IV
COMPARISONS OF THE THRESHOLDS AND THE MAXIMUM VALUES OF e_0

Wordlength	6	7	9	12	16	20	24
Max e_0	2.114e-3	2.12e-4	3.41e-5	2.011e-9	6.74e-13	5.696e-13	4.5856e-13
Threshold	9.375e-1	4.69e-1	1.172e-1	1.465e-2	9.1e-4	5.722e-5	3.58e-6

shown to satisfy [7]

$$\hat{x} = fl(x) = x(1+\epsilon)$$
$$fl(a\ op\ b) = (a\ op\ b)(1+\epsilon), \qquad |\epsilon| \leq u \tag{61}$$

where u is the unit roundoff defined by

$$u = (1/2)\beta^{1-t} \quad \text{for rounded arithmetics}$$

and *op* denotes any of the four arithmetic operations $+$, $-$, $\times$, and $\div$.

6.2.3. Roundoff Analysis: For a QRD RLS systolic array of order p with finite-precision floating point arithmetics, denote the first row of input vector as $(\hat{x}_1, \hat{x}_2, \cdots, \hat{x}_p, \sum_{i=1}^{p}\hat{x}_i + \epsilon_p)$, where $\hat{x}_i = fl(x_i)$, $\epsilon_p = \epsilon(\sum_{i=1}^{p}\hat{x}_i)$, and $|\epsilon| < u$ is a constant,[2] and the second row of input vector as $(\hat{x}'_1, \hat{x}'_2, \cdots, \hat{x}'_p, \sum_{i=1}^{p}\hat{x}'_i + \epsilon_p)$. The content of the first boundary cell is given by

$$\hat{r}_{11} = fl\left(\sqrt{\hat{x}_1^2 + \hat{x}_1'^2}\right) = \sqrt{\hat{x}_1^2 + \hat{x}_1'^2}\,(1+\epsilon) \tag{62}$$

and the rotation parameters are $\hat{c} = fl(\hat{x}_1 / \hat{r}_{11})$ and $\hat{s} = fl(\hat{x}'_1 / \hat{r}_{11})$. The contents of the internal cells can then be obtained as

$$\begin{aligned}\hat{r}_{ij} &= fl\left(fl(\hat{s}\hat{x}'_j) + fl(\hat{c}\hat{x}_j)\right)\\ &= \left[\hat{s}\hat{x}'_j(1+\epsilon) + \hat{c}\hat{x}_j(1+\epsilon)\right](1+\epsilon)\\ &\approx (1+2\epsilon)(\hat{s}\hat{x}'_j + \hat{c}\hat{x}_j), \qquad 1 < j \leq p\end{aligned} \tag{63}$$

and the content of the first cell of the EDA is

$$\begin{aligned}\hat{r}_{1,p+1} &= fl\left(fl\left(\hat{s}\left(\sum_{i=1}^{p}\hat{x}'_i + \epsilon_p\right)\right) + fl\left(\hat{c}\left(\sum_{i=1}^{p}\hat{x}_i + \epsilon_p\right)\right)\right)\\ &\approx \left(\hat{s}\sum_{i=1}^{p}\hat{x}'_i + \hat{c}\sum_{i=1}^{p}\hat{x}_i\right) + 6\epsilon_p.\end{aligned} \tag{64}$$

From (62), (63), and (64), the mismatched τ_1 resulting from the finite precision computation of the first row is given by

$$\tau_1 = 6\epsilon_p - \left(\epsilon\sqrt{\hat{x}_1^2 + \hat{x}_1'^2} + 2\epsilon\sum_{i=2}^{p}\left(\hat{s}\hat{x}'_j + \hat{c}\hat{x}_j\right)\right) \tag{65}$$

and it can be bounded by

$$\begin{aligned}|\tau_1| &\leq 6p|\epsilon x_{\max}| + |2\epsilon x_{\max}| + 4(p-1)|\epsilon x_{\max}|\\ &= (10p-2)|\epsilon x_{\max}| \leq 10p|\epsilon x_{\max}|.\end{aligned} \tag{66}$$

For the second row, with the same principle, the mismatch is bounded by $10(p-1)|\epsilon x_{\max}|$. The total mismatch from the whole array is given by

$$|\tau| \leq \sum_{i=0}^{p-1} 10(p-i)|\epsilon x_{\max}| = 5p(p+1)|\epsilon x_{\max}|. \tag{67}$$

The possible mismatch is thus bounded by

$$|\tau| \leq 5p(p+1)|\epsilon x_{\max}| = |\tau|_{\max}. \tag{68}$$

This bound can be interpreted as: for each row of input, each processing cell contributes about $|\epsilon x_{\max}|$ amount of roundoff error. Since there are about $p(p+1)$ processing cells, the total possible roundoff error is then $p(p+1)|\epsilon x_{\max}|$.

In order to prevent a false alarm, a threshold device is needed at the output of e_0 and the threshold, th, has to be greater or equal to $|\tau|_{\max}$. Suppose $\beta = 2$, $t = 16$, then $u = 2^{-16}$. Given scaled input data such that $|x_{\max}| = 1$, the threshold of a QRD RLS array of order $p = 20$ must satisfy

$$th \geq |\tau|_{\max} \cong 5 \cdot 20 \cdot 21 \cdot 2^{-16} = 0.032. \tag{69}$$

Table IV shows the comparisons of the maximum values of the output residuals e_0 obtained over a period of $n = 10^4$ and $|\tau|_{\max}$ derived from (68) for different wordlength. We can see that the estimated $|\tau|_{\max}$ bound can prevent the false alarm problem. Since the threshold bound is obtained from conservative derivations, it can indeed provide a false alarm free output. However, as shown in Table IV, the estimated threshold bound may be much greater than that of the actual maximum of the residuals. In practice, we may relax the estimated threshold bound from information obtained in previous data to ensure the threshold will not be too high. A higher than necessary threshold may result in a small error size that's not detectable.

6.3. Overall Wordlength Consideration

In order to prevent missing error detection, we want the error size $\Delta = \min(\delta, \eta_j)$ to be as small as possible. While we want to prevent a false alarm, we also want to choose a threshold high enough for a false-alarm-free condition. Both situations cannot be satisfied simultaneously since they are in conflict and some trade-off must be made.

To determine the error size Δ, from (53), (54), and (55), we need the threshold $th \leq \lambda^{2p}\Delta$. Otherwise, the propagated error will be eventually truncated to zero by the threshold device. Accordingly,

$$B_\Delta \leq \lceil -\log_2 th \rceil \tag{70}$$

since a smaller error size is undetectable. From (56), a

[2]To simplify the notation, we do not give indexes to different ϵ's.

criterion to choose B_Δ is then given by

$$\lceil -2p\log_2\lambda - \log_2\Delta \rceil \leqslant B_\Delta \leqslant \lceil -\log_2 th \rceil. \quad (71)$$

If the small error size Δ is chosen in a way such that $\lceil -2p\log_2\lambda - \log_2\Delta \rceil \leqslant \lceil -\log_2 th \rceil$, then we can choose $B_\Delta = \lceil -2p\log_2\lambda - \log_2\Delta \rceil$ and the error size Δ is detectable. However, on the other hand, if $\lceil -2p\log_2\lambda - \log_2\Delta \rceil \geqslant \lceil -\log_2 th \rceil$, then there is no choice but to choose $B_\Delta = \lceil -\log_2 th \rceil$ and the minimal detectable error size becomes $\Delta = \lambda^{-2p} \cdot th$. For a threshold set at $th = 10^{-4}$ as given in (69) and an LS order $p = 50$ and $\lambda = 0.98$, we have $\Delta = 7.54 \cdot 10^{-4}$. However, for a smaller LS order p, a smaller error size can be detected. For example, with $p = 20$, we have $\Delta = 1.5 \cdot 10^{-4}$. To prevent overflow, from (27), the minimum wordlength of the mth row is

$$B_m = \lceil (m-1)(1+\log_2\lambda) + \log_2 \Re \rceil. \quad (72)$$

For a QRD RLS systolic array to detect small error size Δ without false alarm and overflow problems, the minimum wordlength of the mth row should be

$$B_{\min}(m) = \max(B_m, B_\Delta). \quad (73)$$

VII. Conclusions

We presented detailed analysis to show that the rotation parameters of the RLS algorithm based on the Givens rotation method will eventually reach the *quasi-steady-state* if the forgetting factor λ is very close to 1. With this model, the dynamic range of each processing cell can be derived and from this, a proper wordlength can be chosen to ensure correct operations of the algorithm. Our proposed solutions are simple and effective. Simulations have demonstrated that the wordlengths chosen by the proposed dynamic range work very well. Furthermore, we can demonstrate the stability of the QRD RLS algorithm under a finite-precision implementation with this observation. Finally, the missing error detection and false alarm problems are considered based on the results obtained from the model. We presented a design of the wordlength which is overflow-free without missing error detection and false alarm problems.

The results in this paper are of practical importance. Not only can we design a finite-precision QRD RLS systolic array with a minimum wordlength that ensures correct operations, but also provide a fault-tolerant system that can detect a given error size and is false-alarm-free under the quantization effect.

References

[1] M. G. Bellanger, "Computational complexity and accuracy issues in fast least squares algorithms for adaptive filtering," in *Proc. IEEE ISCAS*, pp. 2635–2639, Finland, 1988.

[2] C.-Y. Chen and J. A. Abraham, "Fault-tolerant systems for the computation of eigenvalues and singular values," in *Proc. SPIE*, vol. 696, Advanced Algorithms and Architectures for Signal Processing, pp. 228–237, 1986.

[3] M. J. Chen, "On realizations and performances of least-squares estimation and Kalman filtering by systolic array," Ph.D. dissertation, Electrical Engineering Dept., Univ. California, Los Angles, 1987.

[4] J. M. Cioffi, "The fast adaptive ROTOR's RLS algorithm," *IEEE Trans. Acoust., Speech, Signal Processing*, pp. 631–653, Apr. 1990.

[5] G. D. de Villiers, "A Gentleman–Kung architecture for finding the singular value of a matrix," in *Proc. Int. Conf. Systolic Array*, pp. 545–554, Ireland, 1989.

[6] W. M. Gentleman and H. T. Kung, "Matrix triangularization by systolic arrays," in *Proc. SPIE*, vol. 298, Real Time Signal Processing IV, p. 298, 1981.

[7] G. H. Goloub and C. F. Van Loan, *Matrix Computation*, 2nd ed. Baltimore, MD: Johns Hopkins, 1989.

[8] S. Haykin, *Adaptive Filter Theory*. Englewood Cliffs, NJ: Prentice Hall, 1986.

[9] S. F. Hsieh and K. Yao, "Hyperbolic Gram–Schmidt pseudo-orthogonalization with applications to sliding window RLS filtering," presented at the 24th Ann. Conf. Information Science and System, Princeton University, Mar. 1990.

[10] ____, "Systolic implementation of windowed recursive LS estimation," in *Proc. IEEE ISCAS*, pp. 1931–1934, New Orleans, May 1990.

[11] J.-Y. Jou and J. A. Abraham, "Fault-tolerant matrix arithmetic and signal processing on highly concurrent computing structures," *Proc. IEEE*, vol. 74, pp. 732–741, May 1986.

[12] S. Kalson and K. Yao, "Systolic array processing for order and time recursive generalized least-squares estimation," in *Proc. SPIE*, vol. 564, Real Time Signal Processing VIII, pp. 28–38, 1985.

[13] H. Leung and S. Haykin, "Stability of recursive QRD LS algorithms using finite-precision systolic array implementation," *IEEE Trans. Acoust., Speech, Signal Processing*, vol. 37, pp. 760–763, May 1989.

[14] F. Ling, D. Manolakis, and J. G. Proakis, "A recursive modified Gram–Schmidt algorithm for least-squares estimation," *IEEE Trans. Acoust., Speech, Signal Processing*, vol. ASSP-34, pp. 829–836, Aug. 1986.

[15] K. J. R. Liu and K. Yao, "Gracefully degradable real-time algorithm-based fault-tolerant method for QR recursive least-squares systolic array," in *Systolic Array Processors*, McCanny, McWhirter, and Swartzlander, Eds. UK: Prentice Hall, 1989.

[16] C. J. Anfinson, F. T. Luk, and E. K. Torng, "A novel fault tolerant technique for recursive least squares minimization," in *Proc. SPIE*, vol. 975, 1988.

[17] K. J. R. Liu, S. F. Hsieh, and K. Yao, "Two-level pipelined implementation of systolic block Householder transformations with application to RLS algorithm," to be published in *IEEE Trans. Signal Processing*.

[18] K. J. R. Liu and K. Yao, "Spectral decomposition via systolic triarray based on QR iteration," to be published in *IEEE Trans. Signal Processing*, Jan. 1992.

[19] V. J. Mathews and Z. Xie, "Fixed-point error analysis of stochastic gradient adaptive lattice filters," *IEEE Trans. Acoust., Speech, Signal Processing*, vol. 38, pp. 70–80, Jan. 1990.

[20] J. V. McCanny and J. G. McWhirter, "Some systolic array developments in the United Kingdom," *IEEE Computer*, vol. 20, pp. 51–64, July 1987.

[21] J. G. McWhirter, "Recursive least-squares minimization using a systolic array," in *Proc. SPIE*, vol. 431, Real Time Signal Processing VI, pp. 105–112, 1983.

[22] J. G. McWhirter and T. J. Shepherd, "Systolic array processor for MVDR beamforming," *Proc. Inst. Elec. Eng.*, vol. 136, Pt. F, pp. 75–80, 1989.

[23] I. K. Proudler, J. G. McWhirter, and T. J. Shepherd, "The QRD-based least squares lattice algorithm: Some computer simulations using finite wordlength," in *Proc. IEEE ISCAS*, pp. 258–261, May 1990.

[24] P. S. Lewis, "QR-based algorithms for multichannel adaptive least squares lattice filters," *IEEE Trans. Acoust., Speech, Signal Processing*, vol. 38, pp. 421–432, Mar. 1990.

[25] F. Ling, "Efficient least-squares lattice algorithms based on Givens rotation with systolic array implementation," in *Proc. IEEE ICASSP*, May 1989.

[26] I. K. Proudler, J. G. McWhirter, and T. J. Shepherd, "QRD-based lattice-ladder algorithm for adaptive filtering," in *Proc. Int. Symp. Math. Theory of Networks and Systems*, June 1989.

[27] H. Tsubokawa, H. Kubota, and S. Tsujii, "Effect of floating-point error reduction with recursive least square for parallel architecture," in *Proc. IEEE ICASSP*, pp. 1487–1490, Apr. 1990.

[28] A. J. Viterbi and J. K. Omura, *Principle of Digital Communication and Coding*. New York: McGraw-Hill, 1979.

[29] B. Yang and J. F. Bohme, "Systolic implementation of a general adaptive array processing algorithm," in *Proc. IEEE ICASSP*, pp. 2785–2788, 1988.
[30] J. H. Wilkinson, *The Algebraic Eigenvalue Problem*. New York: Oxford, 1965.

KuoJuey Ray Liu (S'86–M'90) received the B.S. degree in electrical engineering from National Taiwan University and the M.S.E. degree in electrical engineering and computer science from the University of Michigan, Ann Arbor, in 1983 and 1987, respectively, and the Ph.D. degree in electrical engineering from the University of California, Los Angeles, in June 1990.

From 1983 to 1985, he served in the Signal Corps, Taiwan, as a communications officer. Since 1985, he has been a teaching and research assistant at the University of Michigan and UCLA. He is currently an Assistant Professor of electrical engineering, Department and Systems Research Center, University of Maryland, College Park, MD. His research interests include parallel processing algorithms and architectures for signal/image processing and communications, adaptive signal processing, spectral estimation, video signal processing, fault-tolerant computing in VLSI systems, design automation for DSP VLSI systems, and fast algorithms.

Dr. Liu was awarded the President Research Partnership from the University of Michigan in 1987, and the University Fellowship and the Hortense Fishbaugh Memorial Scholarship from UCLA in 1987–88 and 1989, respectively. He was also awarded the Outstanding Graduate Student Award in Science and Engineering from Taiwanese-American Foundation.

Shih-Fu Hsieh (S'87–M'90) received the B.S. degree from the National Taiwan University, Taipei, Republic of China, in 1984, and the M.S., Engineer, and Ph.D. degrees from the University of California, Los Angeles, in 1987, 1989, and 1990, respectively, all in electrical engineering.

From 1984 to 1986 he was an ensign instructor at the Naval Communication and Electronics School, Taiwan. Since 1990 he has been with the National Chiao Tung University, Hsinchu, Taiwan, where he is currently an Associate Professor of Communication Engineering. His current research interests include adaptive signal processing, digital communications, and parallel processing algorithms and architectures.

Kung Yao (S'59–M'65) received the B.S.E. (Highest Honors), M.A., and Ph.D. degrees in electrical engineering from Princeton University, Princeton, NJ, in 1961, 1963, and 1965, respectively.

In 1965–1966, he was an NAS-NRC Post-Doctoral Research Fellow at the University of California, Berkeley. Since 1966, he has been with the University of California, Los Angeles. Presently, he is a Professor in the Electrical Engineering Department. In the fall of 1969, he was a visiting assistant professor at the Massachusetts Institute of Technology and a visiting senior research associate at the NASA Electronics Research Center, Cambridge, MA. In 1973–74, he was a visiting associate professor at Eindhoven Technical University in Eindhoven, The Netherlands. In 1985–1988, he served as an assistant dean of the School of Engineering and Applied Science at UCLA. His research interests include stochastic processes, digital communication theory, satellite communication systems, simulation, radar systems, systolic and VLSI algorithms and systems, and system identification. He is the co-author of *Processing and Algorithm in Communication and Radar Systems*, to be published.

Dr. Yao is a member of Phi Beta Kappa, Sigma Xi, and the American Association for the Advancement of Science. He has served as Program Chairman, Secretary, and Chairman of the IEEE Information Theory Group in Los Angeles and served two terms as a member of the Board of Governors of the IEEE Information Theory Group. He was the Co-Chairman of the 1981 International Symposium on Information Theory held at Santa Monica, CA, and the representative of the IT-BOG in the organization of the 1987 IEEE Information Theory Workshop held at Bellagio, Italy. He was also the Chair of the Technical Program of the 1990 IEEE Workshop on VLSI Signal Processing. He has served as an Associate Editor for Book Reviews of the IEEE TRANSACTIONS ON INFORMATION THEORY and was a member of the editorial board of the journal *Probability in the Engineering and Informational Sciences*, published by the Cambridge Press.

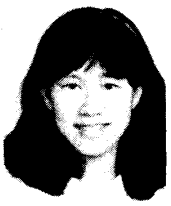

Ching-Te Chiu received the B.S. and M.S. degrees in electrical engineering from National Taiwan University, Taiwan, in 1986 and 1988, respectively. She is currently pursuing the Ph.D. degree in electrical engineering at the University of Maryland, College Park, MD.

Her research experience includes as a summer research student at the Electronics Research Service Organization (ERSO), National Taiwan Institute of Technology, Hsinchu, Taiwan, in 1987. Since 1989, she has been a research assistant in electrical engineering at the University of Maryland, College Park. Her current research interests include signal processing, VLSI architectures and algorithms, image processing, and HDTV systems.